On the Interplay of Nonlinear Interference Generation with Stimulated Raman Scattering for QoT Estimation

On the Interplay of Nonlinear Interference Generation with Stimulated Raman Scattering for QoT Estimation

M. Cantono, *Student Member, OSA*, D. Pilori, *Student Member, OSA*, A. Ferrari, *Student Member, OSA*, C. Catanese, J. Thouras, J.L. Auge, *Member, OSA*, and V. Curri, *Member, IEEE*

***Abstract*—To effectively operate multi-vendor disaggregated networks, performance of physical layer needs to be assessed by a quality-of transmission estimator (QoT-E) delivering *quick* results with a given reliability range. Current state-of-the-art WDM channels are based on multilevel modulation formats relying on DSP-operated coherent receivers, propagating on uncompensated and amplified optical links. In this transmission scenario, beside ASE noise accumulation, nonlinear propagation impairments are well summarized by the accumulation of a Gaussian-distributed disturbance: the nonlinear interference (NLI). When exploiting a transmission bandwidth exceeding the C-band, the interaction of NLI generation with the stimulated Raman scattering (SRS) must be properly considered. We present the derivation of the generalized Gaussian noise (GGN) model for NLI generation, including the SRS and, in general, a spectral and spatial variation of gain/loss. We validate its accuracy by comparing performances predicted by a QoT-E based on the GGN-model with measurements on a testbed exploiting commercial equipment, including 100 Gbps transponders. Considering that operational parameters of commercial equipment are known with a large range of uncertainty, an excellent agreement with errors within 0.5 dB on the generalized SNR is shown, demonstrating that the GGN-model can be used for QoT-E in multi-vendor network scenarios. Moreover, the GGN-model has shown the capability to predict the spectral tilting due to SRS in SNR performances, enabling its application to evaluate the impact of linear pre-tilting for SRS pre-compensation and NLI generation.**

***Index Terms*—NLI, GGN-model, coherent optical systems**

I. Introduction

THE need for optical performance modeling is a request of operators to lower the cost of optical networks by deploying multi-vendor disaggregated optical networks, supporting white boxes and interoperability, while maintaining high performances. To make this effort successful, besides common control models for network elements to be integrated into off-the-shelf controllers, a vendor-agnostic assessment of optical performance is needed to allow controllers to take reasonable decisions. For this reason, operators and vendors are working together to develop vendor-agnostic quality-of-transmission estimators (QoT-Es), as it is demonstrated by consortia such as the Telecom Infra Project (TIP) [1] and Open-ROADM [2]. In fact, the development of these QoT-Es needs to be driven by both operators, vendors and system integrators, as many design and operation aspects need to be agreed on. Such activities have the potential to change the way optical networks are designed and managed, enriching the capabilities of both operators and vendors. Operators will be able to simplify network design deployment by planning for vendor-neutral implementations. Vendors will be able to assess the performance of their products against a tool that is agreed on by the optical community. Practical examples of applications of such QoT-Es include physical-layer control plane definition in multi-vendor and disaggregated optical networks [3] and design, management and orchestration of elastic networks [4], [5]. As for this operations, quick QoT assessments will be needed, performance predictions via numerical solutions of the nonlinear Shrödinger equation are not feasible.

For state-of-the-art transmission techniques based on multilevel modulation formats exploiting polarization-division multiplexing and relying on DSP-operated coherent receivers, it has been extensively shown that nonlinear impairments can be well summarized by the accumulation of a noise-like Gaussian-distributed disturbance named nonlinear interference (NLI), also when exploiting bandwidths exceeding the C-band [6]–[9]. Several models giving an accurate estimate of the NLI accumulation have been proposed in the technical literature and extensively validated by experimental results [10]–[18]. One of the most adopted options for NLI modeling is the Gaussian Noise (GN) model [12], [18] that has been shown to be an effective method to get a quick, yet accurate, conservative prediction of NLI accumulation in commercial systems [5]. For these reasons, the GN-model has been identified as a suitable candidate to be implemented for such QoT-E tools within the TIP consortium [5], [19].

The continuous growth of traffic demand is leading the investigation on optical transmission technologies enabling the increase of the core networks' capacity. In particular, the enlargement of the optical transmission bandwidth beyond the C-band has been proposed as a possible solution to achieve this goal [20]. Nowadays, C+L band systems close to 200 channels on the 50 GHz DWDM grid are gaining traction, and commercial systems with these characteristics are already available on the market [21]. In such ultra-wideband transmission systems – as C+L optical systems – the inter-channel crosstalk due to stimulated Raman scattering (SRS) may induce relevant spectral tilting to be properly considered and compensated for, both taking into account the Amplified

Mattia Cantono, Dario Pilori, Alessio Ferrari, and Vittorio Curri are with DET, Politecnico di Torino, 1029 Torino (TO), Italy. E-mail: mattia.cantono@polito.it)

Clara Catanese, Jordane Thouras, and Jean-Luc Auge are with Orange Labs, France. E-mail: jeanluc.auge@orange.com.

Spontaneous Emission (ASE) noise accumulation and the nonlinear propagation impairments.

Fiber propagation models of state-of-the-art transmission techniques, such as the GN-model, have been derived without considering the simultaneous effect of SRS and NLI generation. This approximation leads to limited inaccuracies typically *absorbed* by system margins where limited bandwidths are exploited and the spectrum is periodically equalized every few spans, as in currently deployed systems. However, not relying on a proper model of joint SRS and NLI generation may cause large inaccuracies with the enlargement of the spectral bandwidth, because of the larger NLI generation in channels at lower frequencies – higher wavelengths – receiving relevant pumping effects. This entails inaccurate performance estimations across the WDM spectrum and an unequal absorption of design margins across the WDM comb, as shown in [22]. Recently, the generalization of the GN-model – the GGN-model – including the effects of SRS and, in general, of a generic spatial and frequency distribution of gain/loss on the generation of NLI in fiber propagation has been proposed in [23]. Other two independent derivations were performed almost simultaneously by two different groups [24], [25] giving similar formulations as the one presented in [23], but no experimental validation has been presented yet.

In this paper, we extend the work presented in [22] with the aim of experimentally validating the use of the GGN-model for QoT-E with commercially available systems, showing how it can be used to safely assess optical performance while taking into account the effect of SRS on NLI estimation. Furthermore, we show an application example of the GGN-model to assess the impact of amplifier tilting for system performance estimation. The experimental results presented in this paper show how the GGN-model can be effectively used in vendor-neutral QoT-Es for the design and control of multi-vendor disaggregated optical networks, as it delivers consistent estimation of QoT performance across the whole WDM spectrum, correctly predicting the slope of SNR vs frequency within a small reliability range of the order of ± 0.5 dB. We also show a comparison with simulative results, where all system parameters are completely under control, contrary to what happens in experimental validation efforts with commercial equipment. This comparison shows that the GGN-model delivers the added value with respect to the GN-model of enabling conservative QoT-E on the entire spectrum, with an overestimation margin that is the same for all wavelengths.

Note that the aim of the GGN-model is not to obtain NLI estimations as close as possible to the real performance like it is done in other models like the Enhanced GN (EGN) model [26]. It indeed aims at being the core module of a *quick* and *safe* QoT-E tool that operates across the full WDM spectrum and that can be reliably used to design and control multi-vendor optical networks, relying on optical systems operating over the entire C-band, and beyond. The GN-model has been proved to be reliable enough for this goal in the center channel of the WDM comb, but it fails to do so across the full WDM comb [22]. This is exactly the gap that the GGN-model aims at filling.

The paper is organized as follows. In Sec. II, we present a detailed derivation of the GGN-model, then in Sec. III the original and extended experimental validation of the GGN-model is presented comparing model results to experimental measurements on a testbed including 100-Gb/s commercial transponders based on PM-QPSK at 32 GBaud. An excellent agreement with errors within 0.5 dB on the generalized SNR is shown for six measured channels. In Sec. IV, we comment on the application of the GGN-model to properly approach the study of linear spectral pre-tilting to counteract the SRS effect and its interaction with NLI generation.

II. The Generalized GN-model

The Generalized GN-model (GGN) model has been proposed in [23], [24], [27] to assess the interplay of NLI generation with spatial and frequency power variations along the fiber. The impact of such generic spatially and frequency distributed loss/gain along the fiber on NLI generation is of special interest when considering full C-band and beyond systems, as SRS-induced inter-channel power crosstalk is not negligible in such transmission scenarios. Specifically, as the optical signal travels through the fiber, a power transfer from higher to lower-frequency spectral components takes place, yielding the well known SRS-induced tilt. For standard single mode fibers (SMF), the efficiency of this phenomenon is maximized for optical signals that are placed approximately 13 THz apart, but it is already visible for total spectral occupations of the order of few THz, corresponding to WDM comb made of at least 40 channels within the standard 50-GHz DWDM grid. Similar spectral distortion effects can be caused by poorly optimized Raman amplified links, where different frequencies undergo different Raman gains, yielding a distortion of the transmitted optical spectrum during propagation. The GGN-model can also be of interest in such scenarios.

SRS in optical communication systems has been widely studied over the last 40 years [28]–[30], and it is well described by a set of coupled differential equations in z – the so-called "pump and probe" equations [29] – describing the power transfer among two continuous wave signals at different frequencies. These equations can be numerically solved to obtain a gain/loss profile that describes how the optical spectrum evolves along the fiber due to the impact of SRS. The same equations can be used to evaluate the distributed spectral-gain of Raman-amplified systems. Although pump and probe equations do not consider modulated signals, they can be safely used in this context as modulation transfer induced by SRS is a second order effect that is averaged out by chromatic dispersion [31], [32]. From a system point of view, SRS-induced effects are well described by normalized amplitude profile functions in both space and frequency. Throughout this paper, we will refer to this as $\rho(z, f)$. As SRS is a nonlinear effect that depends on the PSD of the optical signal, $\rho(z, f)$ depends as well on the PSD of the optical signal traveling into the fiber. The normalized amplitude profile $\rho(z, f)$ can be expressed as a function of the loss/gain profile of the fiber $g(z, f)$ due to losses and SRS-induced effects as:

$$\rho(z, f) = e^{\int_0^z g(\zeta, f)\mathrm{d}\zeta} . \tag{1}$$

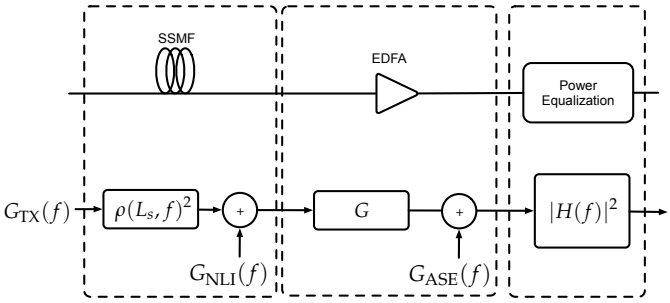

Figure 1. Span equivalent block model for propagation impairment modeling. The fiber attenuates the input PSD and adds NLI noise whose PSD can be computed with the GGN-model.

To study the interplay between these power-variation phenomena and NLI generation in an analytical modeling framework, we extend the well-known Gaussian Noise (GN) model [12], [18], that has been shown to give reasonably conservative predictions to the NLI generation on the center channel well beyond full C-band occupation [6]–[8]. Starting from the GN-model derivation [33], we generalize its formulation considering a generic normalized amplitude profile $\rho(z, f)$ for the optical field, that is a function of both the fiber spatial coordinate z and of frequency f. A similar problem has been addressed in [27], where the authors proxies the impact of $\rho(z, f)$ on NLI by introducing a frequency-dependent effective length used to scale the amount of NLI generated by a fiber having a frequency-flat loss profile. This strategy represents a relatively simple engineering approach to propagation impairment modeling, but it ultimately lacks in precision as recently shown in [22] since the impact of $\rho(z, f)$ over the Four-Wave Mixing (FWM) efficiency is neglected. To overcome such limitation, we include $\rho(z, f)$ in deriving the GN-model as shown in Appendix A. The main result of this is what we define as the GGN-reference formula, describing the power spectral density of the NLI at frequency f at the end of a fiber of length L_s, before amplification. The GGN reference formula is described by Eq. 2 at the bottom of the page. In Eq. 2, $G_{\text{TX}}(f)$ is the PSD of the transmitted channel at frequency f, β_2 and β_3 are the dispersion parameters of the fiber. The key differentiating element in the GGN-model equation with respect to the GN-model is the expression of the FWM efficiency, that in Eq. 2 is expressed by the absolute square of the inner spatial integral made by the product of a phase matching condition with a term expressing the gain/loss at the different frequencies $(f, f_1, f_2, f_1 + f_2 - f)$ referenced in the outer integrals. Eq. 2 can be integrated numerically in few minutes over a standard CPU.

Similarly to the well-known GN-model [18] with incoherent accumulation with fiber spans, Eq. 2 can be used to estimate the total amount of NLI of multi-span links by incoherently adding every single contribution of each span in the link. To this purpose, it is useful to describe a span made of an optical fiber followed by an amplifier and possibly by a power equalization stage referring to the equivalent block scheme of Fig. 1.

The optical fiber is modelled as a filtering block accounting for both SRS-induced tilt and fiber loss, followed by an NLI addition block. Thus, for each fiber we apply a block attenuating the input signal PSD $G_{\text{TX}}(f)$ by a factor $\rho(L_s, f)^2$, followed by the NLI addition. The PSD of this NLI source $G_{\text{NLI}}(f)$ is given by Eq. 2. The amplification stage is modeled by a gain block with gain G followed by the ASE noise addition. We define the PSD of the ASE noise as G_{ASE}. If span transparency is assumed, the amplifier has a gain equal to the fiber nominal loss, i.e., $G_{\text{dB}} = \alpha_{\text{dB}} L_s$ in dB units, where α_{dB} is the fiber attenuation coefficient in dB/km. All frequency-dependent characteristics of the amplifier such as gain ripple and tilt are not considered for sake of simplicity, but they can be easily integrated into this block model. Finally, the optional power equalization stage is modeled as a filter with transfer function $H(f)$. If such filter recovers the ratio between the fiber transfer function $\rho(Ls, f)^2$ and its nominal loss, then $|H(f)|^2 = (10^{-\alpha_{\text{dB}} \frac{L_s}{10}}) \rho(L_s, f)^{-2}$. This equivalent block scheme will be used as reference throughout this paper, both for the experimental validation of the GGN-model and the application example.

III. Experimental Validation

The experimental validation of the GGN-model was performed over the Orange laboratory testbed, depicted in Fig. 2. It consists of 20 spans of 80-km Corning SMF-28e+® optical fiber and is typically used for the performance evaluation of the transponders deployed in Orange networks. A total of 58 channels were configured, 3 of them being current generation 32-Gbaud 100-Gb/s PM-QPSK commercial transponders. The remaining 55 channels are generated from a comb of lasers modulated by two 28 GBaud 100-Gb/s PM-QPSK laboratory transmitters to modulate the odd and even interfering channels. A Wavelength-Selective Switch (WSS) is used at the emission to combine the channel comb with the commercial transponders over the standard 50 GHz DWDM grid and 2 additional equalizers are used during transmission every 6 spans to "flatten" the propagating spectrum. No amplifier pre-tilt or WSS pre-emphasis is applied for the first measurements reported in this section.

Real-time measurements of Q-factor before forward error correction were performed with the commercial

$$G_{\text{NLI}}(L_s, f) = \frac{16}{27}\gamma^2 \rho(z, f)^2 \iint_{-\infty}^{+\infty} G_{\text{TX}}(f_1) G_{\text{TX}}(f_2) G_{\text{TX}}(f_1 + f_2 - f) \left| \int_0^{L_s} \exp(+j4\pi^2 (f_1 - f)(f_2 - f)[\beta_2 + \pi\beta_3 (f_1 + f_2)]\zeta) \frac{\rho(\zeta, f_1)\rho(\zeta, f_1 + f_2 - f)\rho(\zeta, f_2)}{\rho(\zeta, f)} \mathrm{d}\zeta \right|^2 \mathrm{d}f_1 \mathrm{d}f_2 \quad (2)$$

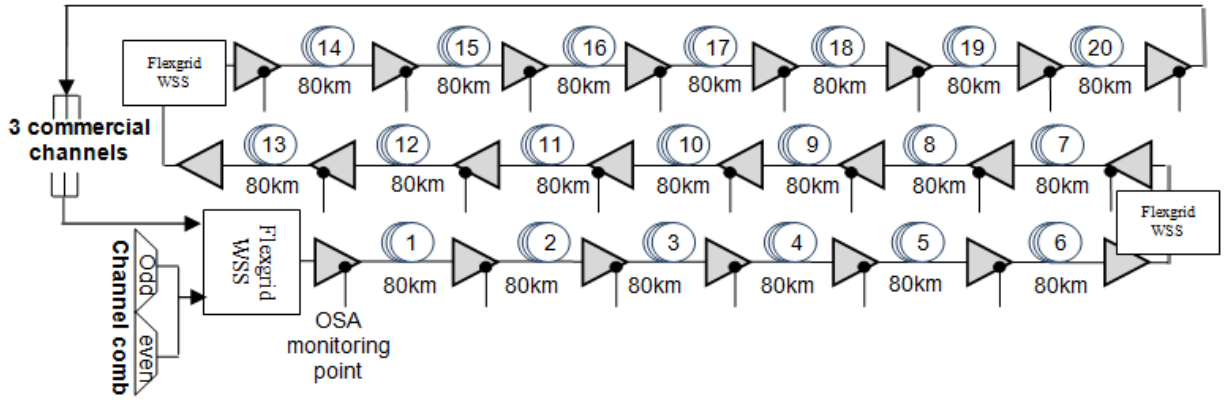

Figure 2. Orange Lab setup.

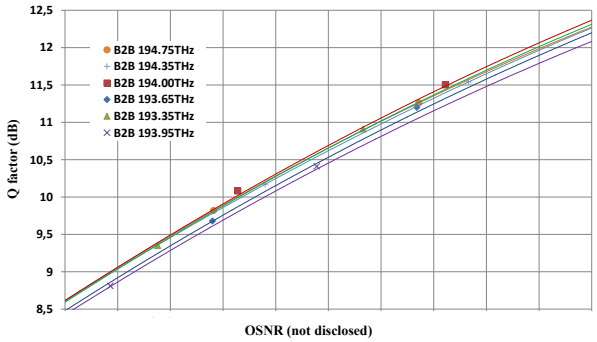

Figure 3. Back to back (B2B) Q-vs-OSNR response of the transponder for all measured frequencies, showing significant performance differences of the commercial devices vs frequency.

32-GBaud transponders, that are typically deployed in Orange networks. The Q-factor is measured by tuning the transponder over 6 different frequencies $[192.95; 193.35; 193.65; 194.00; 194.35; 194.75]$ THz so that the influence of SRS-induced tilting is characterized across the whole C-band. In order to map the measured Q-factors to the generalized signal-to-noise ratio (SNR), the transponder back-to-back response is characterized for each of the 6 frequencies under test at a constant received power of -17 dBm. Results are shown in Fig. 3, where it is shown the measured Q-factor as a function of the measured OSNR. The absolute values of the x-axis are not shown due to nondisclosure agreements with the card manufacturer. Even though the same transponder was used at different laser frequencies, we record significant (up to 0.5 dB) differences in their back-to-back response across the C-band, because of the physical response vs frequency of device components. This emphasizes the need for a well-calibrated setup and controls when assessing performance variation due to propagation impairments over different channels across the full WDM spectrum.

The WDM channel comb was propagated through the 20×80 km link, and the channel power excursions were recorded before each span at the amplifier monitoring port using an Optical Spectrum Analyzer (OSA) (Fig. 4). For this setup, the nominal channel power was close to 0.4 dBm ($+18$ dBm amplifier power), and no power pre-emphasis was applied. The power excursions for all the 58 channels along the first six spans of the testbed are reported in Fig. 4a. The power variations for 3 of the channels under test along the full link are displayed in Fig. 4b: SRS-induced power transfer from higher to lower frequencies is clearly visible as a linear tilt (in dB). Amplifiers ripple are also visible on the side channels of the WDM comb as a nonlinear power variation superimposed to the linear SRS-induced tilt.

In details, measured Q-factors from linecards' interfaces were mapped to generalized signal-to-noise ratio (SNR), which includes both ASE noise and NLI contributions, exploiting the back-to-back characterization of transceivers. While NLI has, in general, a phase-noise component [34], it was found that, under normal operating conditions, such phase noise has a long correlation [26] so that it can be almost completely compensated for by phase recovery circuits implemented in the transponder DSP. This justifies the use of the generalized SNR as a performance metric for fiber propagation impairments, even if it assumes Gaussian-distributed independent NLI components in-phase and quadrature on both polarization states. The nonlinear SNR, $\mathrm{SNR}_{\mathrm{NLI}}$ is defined as:

$$\mathrm{SNR}_{\mathrm{NLI}} = \frac{P_{\mathrm{ch}}}{P_{\mathrm{NLI}}} \tag{3}$$

The experimental values of $\mathrm{SNR}_{\mathrm{NLI}}$ were derived by subtracting the OSNR contribution from the generalized SNR as follows:

$$\mathrm{SNR}^{-1} = \mathrm{OSNR}^{-1} + \mathrm{SNR}_{\mathrm{NLI}}^{-1} \tag{4}$$

where the OSNR, which considers only ASE noise, is measured using an OSA outside signal bandwidth. While the absolute accuracy of the OSNR measurement is difficult to assess, its repeatability was found to be very good with less than ± 0.1 dB variation thanks to automated software control. Also, the validity of the OSNR measurement is good due to the relatively large WDM channel spacing (32 GBaud over a 50 GHz grid), that enables reliable ASE noise probing when the channel under test is turned off. This is also backed up by

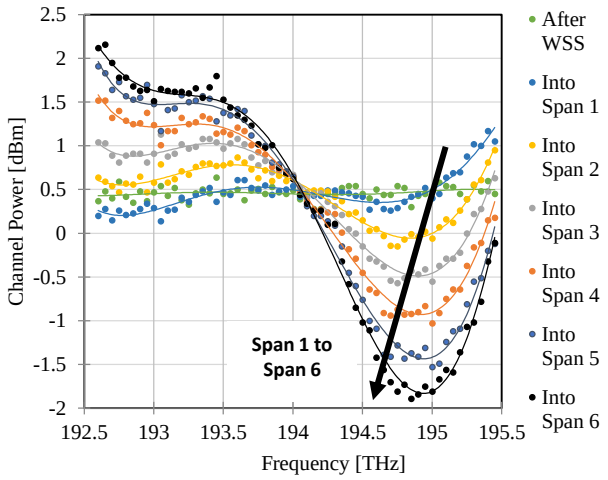

(a) Channels power excursion for the first 6 spans over the Orange testbed. Linear tilt due SRS and a superimposed gain ripple are clearly visible.

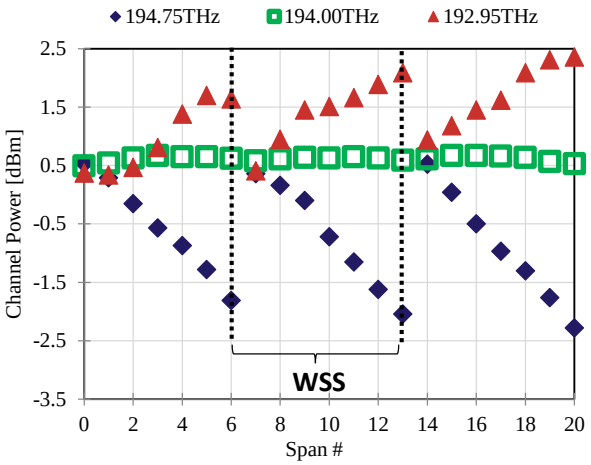

(b) Power per channel evolution for three channels (blue, green and red) at the beginning of each span of the Orange testbed.

Figure 4. Power evolution due to SRS and amplifier ripple along the Orange testbed.

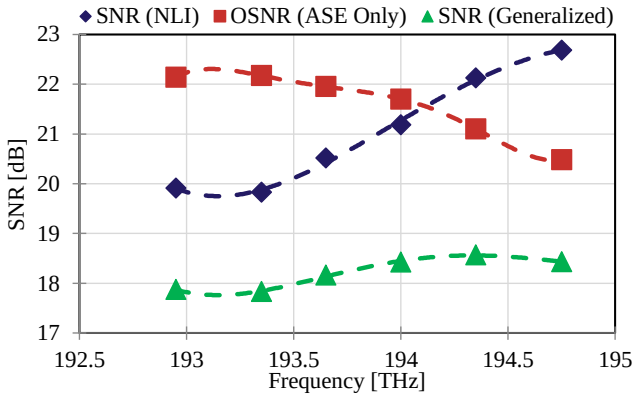

Figure 5. Experimental OSNR, nonlinear SNR and generalized SNR for the 6 measured frequencies. the relative gap between OSNR and nonlinear SNR is non constant due to the interplay between SRS and NLI generation.

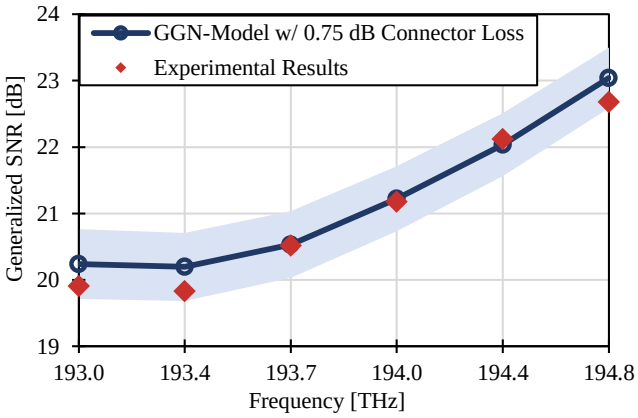

Figure 6. Comparison of experimental and modeled nonlinear SNR. Diamond markers represent experimental results, whereas the solid blue curve is the GGN-model assuming 0.75 dB connector loss. The shaded blue region around the estimations of $\mathrm{SNR}_{\mathrm{NLI}}$ of approximately ± 0.5 dB represents an uncertainty interval mainly caused by connector loss uncertainty.

the fact that NLI is mainly located in-band with respect to the WDM channels [18], allowing for reliable estimation of ASE noise in between channels. Thus, turning off the channel under test makes ASE noise level estimations even more reliable.

The experimental results for generalized SNR, nonlinear SNR and OSNR are reported in Fig. 5, where noise is evaluated over an equivalent optical bandwidth of 0.1 nm ($\sim$ 12.5 GHz). Values of nonlinear SNR show that higher frequency channels benefit from SRS-induced power depletion, which reduces the amount of generated NLI. The opposite happens with lower-frequency channels. The central channels are the best performing ones, even though they are not at the optimum Locally-Optimized Globally Optimized (LOGO) [3] power, being the OSNR equal to the nonlinear SNR, while it should be 3-dB higher. This is caused by these channels experiencing more nonlinear interactions from adjacent channels than those at the edge of the spectrum. This justifies the need for modeling frameworks taking into account SRS-induced tilt in the nonlinear SNR calculation, to derive a more general optimal power settings.

The experimental measurements are plotted in Fig. 6 as red diamond markers, to be compared to the GGN-model predictions. Contrary to validations with simulations or with experimental setups based on research equipment, comparing QoT estimations with measures on a setup made of commercial equipment entails a non-negligible degree of uncertainty in accounting for the exact values of system parameters, such as output power levels, amplifiers working points etc. This is indeed the most challenging aspect of such scenarios, as current generation commercial devices do not provide rigorous characterization data of their operational parameters, nor convenient software interfaces to access this information. Passive devices like optical fibers are even more challenging to characterize in an exact way, as active measurement devices

are needed. These issues get exacerbated also in real field scenarios, where even the type of the deployed fibers might be unknown. Consequently, as of today, a QoT-E based on an analytical model to predict the NLI strength, can only generate results within an inaccuracy bar whose width depends on the precision in the knowledge of real system parameters.

For the considered experimental testbed, the most critical piece of information is related to the power levels of each channel at the input of each fiber due to the unknown value of the fiber connector loss, having a typical value in between 0.5 to 1 dB. Characterizing the connector loss is impractical: using FC-APC angular connectors, the loss may change every time the connector is unscrewed for characterization. For this reason, connector losses are not measured in the setup. An uncertainty on the power levels entering the fiber entails an uncertainty on the estimation of the NLI strength and SNR_{NLI}. A degree of uncertainty is also associated with fiber parameters. However, their impact on SNR_{NLI} estimation error is smaller than the one associated with power levels uncertainty. For this comparison, we used datasheet fiber parameters for SMF-28e+® with a polarization-averaged Raman efficiency [35] $C_r = 0.39$ 1/W/km. In order to take into account the strong ripple effects exhibited by the line amplifiers (see Fig. 4a), we inserted into Eq. 2 the exact spectrum levels derived from OSA measurements. The measured power profiles were also used to numerically estimate SRS crosstalk, deriving $\rho(L_s, f)^2$ for each span starting from the well-known pump-and-probe equations describing SRS [29]. The estimated SRS tilt is well matched with the experimental data. To understand the impact of connector loss uncertainty on SNR_{NLI}, we computed the GGN-model for three different values of connector loss, i.e. 0.5 dB, 0.75 dB, and 1.0 dB. The value that best-matched the GGN-model with the experimental SNR_{NLI} results is 0.75dB. The GGN-model estimation for this connector loss value is reported with the solid circle-marked curve in Fig. 6. The other two values define a range around the best estimation of approximately ± 0.5 dB that is reported in Fig. 6 with the blue shaded region, to visually convey the information of the variability of the QoT estimations due to system parameters uncertainty. From Fig. 6 it is evident how the experimental results fall within the shaded region around the GGN-model, that assuming a 0.75 dB loss yields an average estimation error across the 3 different channels around 0.3 dB. The most important characteristic of the GGN-model is however represented by the fact that the slope of nonlinear SNR is correctly estimated by the GGN-model, thus the GGN-model can be safely used to estimate performance over the full WDM-comb. It should also be highlighted in this scenario the GGN-model estimations are not conservative with respect to experimental data due to the aforementioned system parameters uncertainty eroding such conservative margin. Later, in Sec. IV, an example of application will be compared against full split step simulation, where *full control* of system parameters is possible. In this scenario, the conservative nature of the GGN-model will emerge clearly.

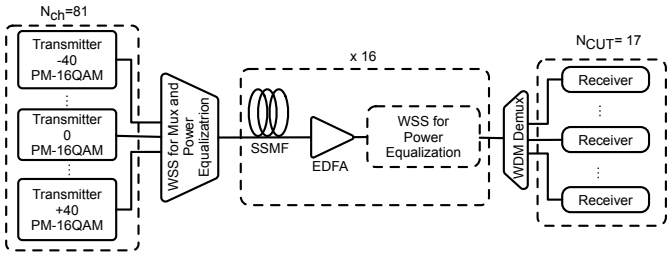

Figure 7. System setup for the GGN-model example of application.

Table I
SIMULATED FIBER PARAMETERS

Parameter	Value
Span length	$L_{\text{s}} = 100$ km
Number of spans	$N_{\text{s}} = 16$
Attenuation	$\alpha_{\text{dB}} = 0.2$ dB/km
Chromatic dispersion	$D = 16.7$ ps/nm/km
nonlinear coefficient	$\gamma = 1.3$ 1/W/km
Polarization Averaged Raman Efficiency [35]	$C_r = 0.39$ 1/W/km

IV. ASSESSING THE IMPACT OF POWER TILTING STRATEGIES WITH THE GGN-MODEL

In this section, an example of application of the GGN-model is presented. Specifically, we show how the GGN-model can be used to assess the impact of power pre-emphasis through amplifier tilting on channel performance in wide-band optical communication systems. This effort is motivated by the fact that experimental measurements performed over the Orange testbed described in Sec. III showed an improvement in channel SNR when applying power pre-emphasis via amplifier tilting. Specifically, a -1.2 dB tilt showed up to 0.3 dB gain in SNR, even though amplifiers ripple gets worse as the gain is non-flat anymore. Starting from this preliminary qualitative results, we used the model to test the effectiveness of pre-tilt in the generalized SNR.

For this task, we considered a system, different from the experimental setup of the previous section, made of 81 WDM channels. Each WDM channel is modulated with a PM-16QAM signal at 32 GBaud with raised cosine spectra with 15% roll-off, and transmitted over 16 100-km spans of standard SMF, with typical fiber parameters as reported in Tab. I. The channels are spaced on the standard DWDM grid (50 GHz), obtaining a total modulated optical bandwidth of $B_{\text{WDM}} \approx 4$ THz (full C-band). The nominal launch power per channel is -0.8 dBm. At the end of each span, an EDFA with noise factor $F = 5$ dB fully recovers span loss and applies a tilt to counteract the effect of SRS. No gain ripple is considered in this section. Every 4 span a WSS equalizes the power of each WDM channel.

At first, we calculated the power profile spatial evolution before each WSS caused by SRS crosstalk of the full WDM spectrum without any EDFA gain tilting. To do so, we solved numerically the pump-and-probe coupled equations [29] for SRS. After 4 spans, the SRS-induced tilting was of the order of 2 dB. We considered this measurement as the baseline

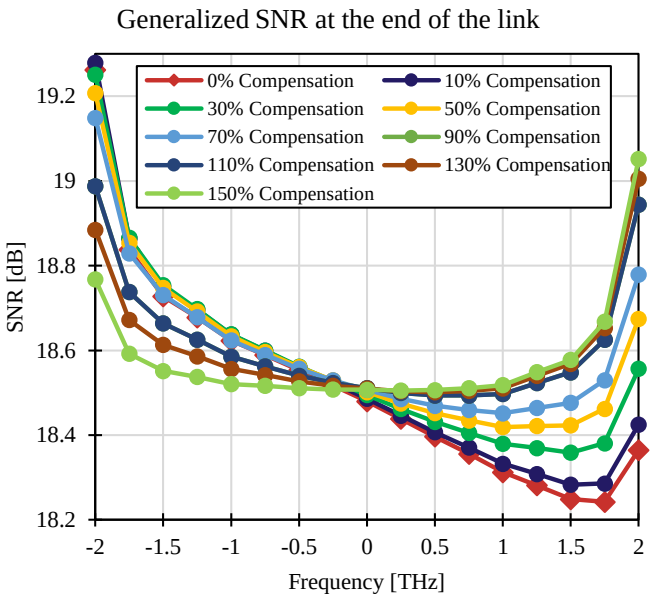

Figure 8. SNR vs pre-compensation percentage. Results obtained with the GGN-model.

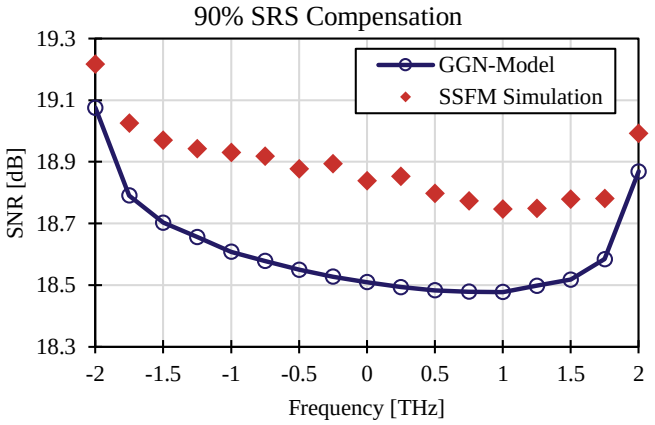

Figure 9. Comparison between the GGN-model and a full split-step simulation for 90% pre-compensation.

reference to compute tilt profiles for compensation. Then, we considered different percentages of the inverse of this tilt deriving different profiles to test. Each profile is equally distributed across every EDFA in between two WSS. For instance, 0% pre-compensation means that the EDFA gain profile is flat and the SRS-induced tilting is compensated only at each WSS. On the other end, 100% pre-compensation means that each EDFAs pre-compensate 25% of the overall SRS tilting, obtaining an almost flat power profile at the beginning of each WSS.

On Fig. 8 we show the generalized SNR of 17 WDM channels computed over a 12.5 GHz equivalent noise bandwidth, equally spaced across the total WDM comb, with different percentages of pre-compensation, estimated with the GGN-model. It can be noted that with no compensation, the generalized SNR shows approximately a 1 dB tilt in SNR. As pre-compensation is applied, the SNR tilt reduces: lower frequency channels undergo a decrease in generalized SNR, whereas higher frequency ones an improvement. At 90% compensation, a 0.3 dB improvement in the worst SNR channel is achieved. At 150% pre-compensation, i.e. with a 50% overcompensation, overall SNR flatness is reached, but there is a slight decrease in minimum SNR with respect to the 130% case.

To validate these GGN-model results, we set up a numerical split step Fourier method (SSFM) based simulation using the Fast Fiber Simulator Software (FFSS) [36]. In order to simulate SRS, we modify the SSFM of the FFSS by introducing, in each linear step a non-flat gain/loss profile to be applied to the optical field. Such profile is obtained by solving the pump and probe equations for SRS [29]. This approach represents a simplified way of taking into account SRS into an SSFM based simulator, as it neglects all time-dependent related SRS effects such as cross-gain modulation and relative intensity noise transfer. Such assumption is however reasonable, considering that time-dependent SRS effects can be well-modeled with an equivalent noise transfer from high frequencies to lower ones. The characteristics of such transfer are governed by a low-pass transfer function with corner frequency much smaller than 500 MHz, as chromatic dispersion averages out higher frequencies [31], [32]. Thus, for channels with optical bandwidths much larger than such frequency value, as the simulated ones, the additional impairment is irrelevant. In particular, we focus on the simulative validation of the GGN-model with a 90% pre-compensation equally distributed across every EDFA in between WSSs. The 17 WDM channels-under-test (CUT) were generated with 12 repetitions of different 2^{14} PRBS sequences, while the other channels were generated with random PM-16QAM symbols. At the receiver, each CUT is independently filtered with a fully-data-aided 17-tap LMS adaptive equalizer, then the generalized SNR is evaluated directly on the received constellation. No phase recovery is applied since lasers are assumed ideal.

Simulation results, compared with predictions of the GGN-model, are shown in Fig. 9. The GGN-model once again is in a good agreement with simulation results, correctly estimating the slope of the SNR across all channels. It should be noted that the model estimations show a *conservative* 0.2 dB gap from simulation results across all WDM comb. This is due to the well-known conservative assumption made by the GN-models family of having Gaussian signals being propagated along the fiber link [18]. As widely discussed in literature [12], [18], this is a conservative assumption, as at the beginning of the optical link such hypothesis does not hold, therefore the GN-models tend to moderately overestimate NLI at the beginning of link propagation. As discussed in the Sec. III, such conservative gap is displayed only in simulative results as it is possible to *exactly* control all system parameters playing a role in NLI estimation. Discussing optimality of different compensation strategies is out of the scope of this paper, but it is worth stressing that the GGN-model can be considered as a key enabler to achieve such goal.

V. Conclusions

In this paper, we have first revised the derivation of the generalized Gaussian noise model to properly estimate the NLI accumulation within a QoT-E needed to effectively operate disaggregated multi-vendor network. The GGN-model generalizes the GN-model by taking into account the effect of SRS and of spatial/frequency amplitude variations in the fiber in modeling NLI generation, so it is needed when exploiting the full C-band and beyond.

For the first time, we validated the use of the GGN-model within a QoT-E by comparing its predictions to measurements on six channels generated by commercial 100-Gb/s transponders on the testbed at the Orange laboratories based on commercial equipment. The validation has shown an excellent agreement between the QoT-E predictions and measurements, that quantitatively enables a QoT-E reliability range of ± 0.5 dB for all the measured channels. It means that in this setup, exploiting the GGN-model-based Qot-E predictions, lightpaths could be deployed with a margin limited to 0.5 dB, independently of the spectral placement within the transmission bandwidth. Therefore, results of the experimental validation encourage the adoption of the GGN-model in QoT-E modules needed in multi-vendor networks for design and orchestration, as it is able to deliver QoT estimations that are consistent across the full WDM spectrum. To this purpose, additional work is needed to derive an approximated closed-form for the GGN-model, following the same approach adopted in [18] used to obtain an approximation to the GN-model.

We have also shown an application of the GGN-model to assess the impact of linear spectral pre-tilting to counteract the SRS effect and NLI generation. Besides its use within the QoT-E framework, the GGN-model could be fruitfully used in future works to extend the concept of LOGO control plane [3] introducing a frequency dependent power setting. As a final note, we remark that the GGN-model – as the GN-model – is not aiming at the *exact* NLI prediction, but at a *quick* NLI evaluation for QoT-E, to enabling deployment of lightpaths with a predefined and reliable limited margin.

Acknowledgment

The authors would like to thank N. Brochier and S. Gauthier for their help in setting up the measurement testbed.

Appendix
The Derivation of the GGN-model

The derivation of the GGN-model follows the method already exploited in deriving the GN-model detailed described in [33], so assuming to analyze propagation of Gaussian distributed spectral components. Then, in addition to [33] hypotheses, we suppose frequency/space variation of power profile in fiber spans. As in [33], we develop the model exploiting the single-polarization wave equation in fibers – the nonlinear Schrödinger equation (NLSE) – then, we generalize the results including polarization relying on the Manakov equation (ME), i.e., on the dual-polarization NLSE with random birefringence – and consequent PMD effect – averaged out. It has been shown that the ME can be reliably used far beyond its validity bandwidth in case of propagation of Gaussian distributed and depolarized signals [8] and for polarization division multiplexed channels with multilevel modulation formats [9]. This will be the validity scenario for the GGN-model.

The nonlinear Schrödinger equation (NLSE), in the frequency domain, has the following form:

$$\partial_z E(z,f) = \left[g(z,f) - j\beta(f)\right] E(z,f) + Q_{\text{NLI}}(z,f) \quad (5)$$

where z is the propagation direction, $E(z,f)$ is the Fourier transform of the propagating modal amplitude, ∂_z is the partial derivative of $E(z,f)$ with respect to z, $\beta(f)$ is the dispersion coefficient, $g(z,f)$ is the profile of amplitude evolution of modal amplitude that may vary with respect to both z and f, $Q_{\text{NLI}}(z,f)$ is the nonlinear term determined by the Kerr effect that is given by:

$$Q_{\text{NLI}}(z,f) = -j\gamma E(z,f) * E^*(z,-f) * E(z,f)\ . \quad (6)$$

where "$*$" is the convolution operator. according to the theory of differential equation, the formal solution of Eq. 5, i.e., of the evolution of the Fourier transform of the modal amplitude vs. z, has the following form:

$$E(z,f) = e^{\Gamma(z,f)} \int_0^z e^{-\Gamma(\zeta,f)} Q_{\text{NLI}}(\zeta,f)\mathrm{d}\zeta \ + \ e^{\Gamma(z,f)} E(0,f) \quad (7)$$

where $\Gamma(z,f)$ is given by:

$$\Gamma(z,f) = \int_0^z -j\beta(f) + g(\zeta,f)\mathrm{d}\zeta = -j\beta(f)z + \int_0^z g(\zeta,f)\mathrm{d}\zeta \quad (8)$$

We can subdivide $E(z,f)$ solution of Eq. 7 as the sum of two components: $E_{\text{LIN}}(z,f)$ considering linear propagation effects only ($g(z,f) - j\beta(f)$), and $E_{\text{NLI}}(z,f)$ considering the impairment of Kerr effect and its interaction with linear propagation. Therefore,

$$E(z,f) = E_{\text{NLI}}(z,f) + E_{\text{LIN}}(z,f)\ , \quad (9)$$

where the linear component $E_{\text{LIN}}(z,f)$ is:

$$E_{\text{LIN}}(z,f) = e^{\Gamma(z,f)} E(0,f)\ , \quad (10)$$

and the nonlinear component $E_{NLI}(z,f)$ is:

$$E_{\text{NLI}}(z,f) = e^{\Gamma(z,f)} \int_0^z e^{-\Gamma(\zeta,f)} Q_{\text{NLI}}(\zeta,f)\mathrm{d}\zeta \quad (11)$$

In general, the formal solution of Eq. 7 for the modal amplitude evolution is useful to observe the two contributes – linear and nonlinear – to propagation impairments, but cannot be practically exploited, because the unknown function $E(z,f)$ is also in the right side term of Eq. 7 being the cause of $Q_{\text{NLI}}(z,f)$ as clearly displayed by Eq. 6.

A. Perturbative Approach on the nonlinear Impairment

In silica fibers, the strength of Kerr effect is much less intense of impairments of linear propagation, mainly given by chromatic dispersion. So, we are legitimate to exploit a perturbative approach for which $E_{\text{NLI}}(z,f)$ is indeed a

perturbation of $E_{\text{LIN}}(z,f)$. Consequently, we may assume that the nonlinear term defined in Eq. 6 is induced only by the linear component $E_{\text{LIN}}(z,f)$ of the modal amplitude $E(z,f)$. Such an approximation yields to not considering the second-order effects, i.e., the nonlinear effects induced by $E_{\text{NLI}}(z,f)$. So, practically, the perturbative approach implies to use the following form for $Q_{\text{NLI}}(z,f)$ in place of the *exact* one of Eq. 6:

$$Q_{\text{NLI}}(z,f) = -j\gamma E_{\text{LIN}}(z,f) * E^*_{\text{LIN}}(z,-f) * E_{\text{LIN}}(z,f)\ . \tag{12}$$

As the convolution operator is defined as:

$$x(t) * h(t) = \int_{-\infty}^{\infty} x(\tau)h(t-\tau)\mathrm{d}\tau\ , \tag{13}$$

we can expand Eq. 12 in the following form:

$$\begin{aligned}
&Q_{\text{NLI}}(z,f) = \\
&= -j\gamma \left[\int_{-\infty}^{+\infty} e^{\Gamma(z,f_1)} e^{\Gamma^*(z,f_1-f)} E(0,f_1)E^*(0,f_1-f)\mathrm{d}f_1\right] * \\
&\quad * \left[e^{\Gamma(z,f)}E(0,f)\right] &(14)\\
&= -j\gamma \iint_{-\infty}^{+\infty} e^{\Gamma(z,f_1)} e^{\Gamma^*(z,f_1-f_2)} e^{\Gamma(z,f-f_2)}\cdot \\
&\quad \cdot E(0,f_1)E^*(0,f_1-f_2)E(0,f-f_2)\mathrm{d}f_1\mathrm{d}f_2 &(15)\\
&= -j\gamma \iint_{-\infty}^{+\infty} e^{\Gamma(z,f_1)+\Gamma^*(z,f_1-f_2)+\Gamma(z,f-f_2)}\cdot \\
&\quad \cdot E(0,f_1)E^*(0,f_1-f_2)E(0,f-f_2)\mathrm{d}f_1\mathrm{d}f_2 &(16)\\
&= -j\gamma \iint_{-\infty}^{+\infty} A(z,f)\cdot \\
&\quad \cdot E(0,f_1)E^*(0,f_1-f_2)E(0,f-f_2)\mathrm{d}f_1\mathrm{d}f_2 &(17)
\end{aligned}$$

where $A(z,f)$ is:

$$\begin{aligned}
&A(z,f) = \\
&= \exp\Bigg(\int_0^z -j[\beta(f_1)-\beta(f_1-f_2)+\beta(f-f_2)]+ \\
&\quad + [g(\zeta,f_1)+g(\zeta,f_1-f_2)+g(\zeta,f-f_2)]\mathrm{d}\zeta\Bigg)\ . &(18)
\end{aligned}$$

Then, inserting Eq. 8 in Eq. 11 we get the following expression for the perturbation $E_{\text{NLI}}(z,f)$:

$$\begin{aligned}
&E_{\text{NLI}}(z,f) = \\
&= e^{-j\beta(f)z} e^{\int_0^z g(\zeta,f)\mathrm{d}\zeta}\cdot \\
&\quad \cdot \int_0^z e^{j\beta(f)} e^{-\int_0^\zeta g(z_1,f)\mathrm{d}z_1} Q_{\text{NLI}}(\zeta,f)\mathrm{d}\zeta \\
&= e^{-j\beta(f)z} e^{\int_0^z g(\zeta,f)\mathrm{d}\zeta} I(z,f) &(19)
\end{aligned}$$

where $I(z,f)$ is:

$$\begin{aligned}
&I(z,f) = \\
&= -j\gamma \iint_{-\infty}^{+\infty} E(0,f_1)E^*(0,f_1-f_2)E(0,f-f_2) \\
&\quad \int_0^z \exp(+j\beta(f)\zeta) \\
&\quad A(\zeta,f)\exp\left(-\int_0^\zeta g(z_1,f)\mathrm{d}z_1\right)\mathrm{d}\zeta\mathrm{d}f_1\mathrm{d}f_2 &(20)
\end{aligned}$$

Substituting in Eq. 19 the expression of $I(z,f)$ we obtain the following expression for the nonlinear perturbation introduced by the Kerr effect:

$$\begin{aligned}
&E_{\text{NLI}}(z,f) = \\
&= e^{-j\beta(f)z} e^{\int_0^z g(\zeta,f)\mathrm{d}\zeta} I(z,f) \\
&\quad - j\gamma \iint_{-\infty}^{+\infty} E(0,f_1)E^*(0,f_1-f_2)E(0,f-f_2) \\
&\quad \int_0^z \exp(+j\beta(f)\zeta) \\
&\quad A(\zeta,f)\exp\left(-\int_0^\zeta g(z_1,f)\mathrm{d}z_1\right)\mathrm{d}\zeta\mathrm{d}f_1\mathrm{d}f_2\ . &(21)
\end{aligned}$$

Note that Eq. 21 relies on the only approximation of Kerr effect being a perturbation of linear propagation and does include frequency/space variations of loss and gain as $g(\zeta,f)$ in addition to frequency variations of the propagation constant $\beta(f)$.

B. NLI Power Spectral Density

In this section, we rely on the same signal form – depolarized and Gaussian signals – and follow the same procedure of [33] to derive the power spectral density $G_{\text{NLI}}(z,f)$ of $E_{\text{NLI}}(z,f)$, that is assumed to be a Gaussian random process. Specifically, using Eq. 16 of [33], one can write the NLI field as

$$\begin{aligned}
&E_{\text{NLI}}(z,f) = -j\gamma f_0^{\frac{3}{2}} e^{-j\beta(f)z} e^{\int_0^z g(\zeta,f)\mathrm{d}\zeta}\cdot \\
&\sum_{i=-\infty}^{+\infty} \delta(f-if_0) \sum_{m,n,k\in\widetilde{A}_i} \sqrt{G_{\text{TX}}(mf_0)G_{\text{TX}}(nf_0)G_{\text{TX}}(kf_0)}\cdot \\
&\xi_m\xi_n^*\xi_k \int_0^z \exp[-\Gamma(\zeta,(m-n+k)f_0)+\Gamma(\zeta,mf_0)+ \\
&+\Gamma^*(\zeta,nf_0)+\Gamma(\zeta,kf_0)]\mathrm{d}\zeta &(22)
\end{aligned}$$

where f_0 is a divider of the symbol rate, ξ is a complex Gaussian random variable and $\delta(f)$ is the Dirac delta function. $\widetilde{A}_i$ represents the set of all triples (m,n,k) such that $m-n+k=i$ and $m\neq n$ or $k\neq n$. This set identifies all non degenerate fourwave mixing components, as detailed in [33]. Following the same averaging procedure of Sec. IV (D) of [33], one obtains the following expression for the single polarization expression of the power spectral density of the NLI noise, i.e.

$$\begin{aligned}
&G^{sp}_{\text{NLI}}(z,f) = 2\gamma^2 f_0^3 \left|\exp\left[\int_0^z g(\zeta,f)\mathrm{d}\zeta\right]\right|^2 \cdot \\
&\sum_{i=-\infty}^{+\infty} \delta(f-if_0) \sum_m \sum_k G_{\text{TX}}(mf_0)G_{\text{TX}}(kf_0)\cdot \\
&G_{\text{TX}}((m-i+k)f_0) \int_0^z \exp[-\Gamma(\zeta,if_0)+ \\
&+\Gamma(\zeta,mf_0)+\Gamma^*(\zeta,(m-i+k)f_0)+\Gamma(\zeta,kf_0)]\mathrm{d}\zeta &(23)
\end{aligned}$$

Similarly, considering a dual polarization signal, following the exact derivation of the previous section and the averaging procedure of Sec.IV (E) in [33] one can write the PSD of the NLI noise generated by dual-polarization signals as

$$G_{\text{NLI}}(z,f) = \frac{16}{27}\gamma^2 f_0^3 \left|\exp\left[\int_0^z g(\zeta,f)\mathrm{d}\zeta\right]\right|^2 \cdot \sum_{i=-\infty}^{+\infty} \delta(f-if_0) \sum_m \sum_k G_{\text{TX}}(mf_0)G_{\text{TX}}(kf_0)\cdot G_{\text{TX}}((m-i+k)f_0)\int_0^z \exp[-\Gamma(\zeta,if_0)+ + \Gamma(\zeta,mf_0)+\Gamma^*(\zeta,(m-i+k)f_0)+\Gamma(\zeta,kf_0)]\mathrm{d}\zeta \quad (24)$$

Then, taking the limit of Eq. 24 for $f_0 \to 0$, such expression can be written as:

$$G_{\text{NLI}}(z,f) = = \frac{16}{27}\gamma^2 \left|e^{\int_0^z g(\zeta,f)\mathrm{d}\zeta}\right|^2 \cdot \cdot \iint_{-\infty}^{+\infty} G_{\text{TX}}(f_1)G_{\text{TX}}(f_2)G_{\text{TX}}(f_1+f_2-f)\cdot \cdot \left|\int_0^z e^{+j[\beta(f_1+f_2-f)-\beta(f_1)+\beta(f)-\beta(f_2)]\zeta} \cdot \cdot e^{+\int_0^\zeta g(z_1,f_1)-g(z_1,f)+g(z_1,f_2)+g(z_1,f_1+f_2-f)\mathrm{d}z_1}\mathrm{d}\zeta\right|^2 \cdot \cdot \mathrm{d}f_1\mathrm{d}f_2 \,. \quad (25)$$

To compact the expression, we introduce the following function $\rho(z,f)$ that considers the evolution of the modal amplitude vs. z for each spectral component f:

$$\rho(z,f) = e^{\int_0^z g(\zeta,f)\mathrm{d}\zeta} \,. \quad (26)$$

This expression may include the effect of frequency variation of loss coefficient, of SRS-induced crosstalk and of distributed amplifications applied to a limited portion of the exploited WDM spectrum.

Exploiting the linearity of the integral operator and the properties of the exponential function, we can rewrite the Eq. 25 as:

$$G_{\text{NLI}}(z,f) = = \frac{16}{27}\gamma^2 \rho(z,f)^2 \cdot \cdot \iint_{-\infty}^{+\infty} G_{\text{TX}}(f_1)G_{\text{TX}}(f_2)G_{\text{TX}}(f_1+f_2-f)\cdot \cdot \left|\int_0^z e^{+j[\beta(f_1+f_2-f)-\beta(f_1)+\beta(f)-\beta(f_2)]\zeta} \cdot \cdot \frac{\rho(\zeta,f_1)\rho(\zeta,f_1+f_2-f)\rho(\zeta,f_2)}{\rho(\zeta,f)}\mathrm{d}\zeta\right|^2 \mathrm{d}f_1\mathrm{d}f_2 \,. \quad (27)$$

Finally obtaining the following expression for the NLI PSD that is the also the final expression of the generalized Gaussian noise model for NLI generated by a single fiber span.

$$G_{\text{NLI}}(z,f) = = \frac{16}{27}\gamma^2 \rho(z,f)^2 \iint_{-\infty}^{+\infty} G_{\text{TX}}(f_1)G_{\text{TX}}(f_2)G_{\text{TX}}(f_1+f_2-f)\cdot \cdot \left|\int_0^z e^{+j\Delta\beta(f_1,f_2,f)\zeta}\Delta\rho(z,f,f_1,f_2)\mathrm{d}\zeta\right|^2 \mathrm{d}f_1\mathrm{d}f_2 \quad (28)$$

where $\Delta\rho$ is given by

$$\Delta\rho(z,f,f_1,f_2) = \frac{\rho(\zeta,f_1)\rho(\zeta,f_1+f_2-f)\rho(\zeta,f_2)}{\rho(\zeta,f)} \quad (29)$$

The use of Eq. 28 in multi-span links is straightforward as for the GN-model. and $\Delta\beta$

$$\Delta\beta(z,f,f_1,f_2) = [\beta(f_1+f_2-f)-\beta(f_1)+\beta(f)-\beta(f_2)]z \quad (30)$$

that can be further expanded as

$$\Delta\beta(z,f,f_1,f_2) = 4\pi^2(f_1-f)(f_2-f)[\beta_2+\pi\beta_3(f_1+f_2)]z \quad (31)$$

as detailed described in Eq. G.2 of [33]. Eq. 28 can be also expanded to be used with coherent accumulation with spans inserting the "phased-array" factor or rely on the incoherent accumulation simply adding up independently NLI generated by each fiber span.

REFERENCES

[1] The Telecom Infra Project (TIP). [Online]. Available: https://telecominfraproject.com

[2] Open ROADM MSA. [Online]. Available: http://www.openroadm.org

[3] P. Poggiolini, G. Bosco, A. Carena, R. Cigliutti, V. Curri, F. Forghieri, R. Pastorelli, and S. Piciaccia, "The LOGON strategy for low-complexity control plane implementation in new-generation flexible networks," in *Optical Fiber Communication Conference/National Fiber Optic Engineers Conference 2013*. The Optical Society, 2013.

[4] V. Curri, M. Cantono, and R. Gaudino, "Elastic All-Optical Networks: a New Paradigm Enabled by the Physical Layer. How to Optimize Network Performances?" *Journal of Lightwave Technology*, vol. PP, no. 99, pp. 1–1, 2017.

[5] G. Grammel, V. Curri, and J. L. Auge, "Physical Simulation Environment of The Telecommunications Infrastructure Project (TIP)," in *Submitted to Optical Fiber Communication Conference/National Fiber Optic Engineers Conference 2018*, 2018.

[6] R. Pastorelli, G. Bosco, A. Carena, P. Poggiolini, V. Curri, S. Piciaccia, and F. Forghieri, "Investigation of the dependence of non-linear interference on the number of WDM channels in coherent optical networks," in *Proc. 38th European Conf. and Exhibition Optical Communications*, Sep. 2012, pp. 1–3.

[7] D. J. Elson, G. Saavedra, K. Shi, D. Semrau, L. Galdino, R. Killey, B. C. Thomsen, and P. Bayvel, "Investigation of bandwidth loading in optical fibre transmission using amplified spontaneous emission noise," *Opt. Express*, vol. 25, no. 16, pp. 19 529–19 537, Aug 2017. [Online]. Available: http://www.opticsexpress.org/abstract.cfm?URI=oe-25-16-19529

[8] G. Saavedra, M. Tan, D. J. Elson, L. Galdino, D. Semrau, M. A. Iqbal, I. Phillips, P. Harper, N. MacSuibhne, A. Ellis, D. Lavery, B. C. Thomsen, R. Killey, and P. Bayvel, "Experimental Investigation of Nonlinear Signal Distortions in Ultra-Wideband Transmission Systems," in *Optical Fiber Communication Conference 2017*. OSA, 2017, p. W1G.1.

[9] M. Cantono, D. Pilori, A. Ferrari, A. Carena, and V. Curri, "Observing the Interaction of PMD with Generation of NLI in Uncompensated Amplified Optical Links," in *2018 Optical Fiber Communication Conference*, 2018.

[10] V. Curri, A. Carena, P. Poggiolini, G. Bosco, and F. Forghieri, "Extension and validation of the GN model for non-linear interference to uncompensated links using Raman amplification," *Opt. Express*, vol. 21, no. 3, pp. 3308–3317, Feb 2013. [Online]. Available: http://www.opticsexpress.org/abstract.cfm?URI=oe-21-3-3308

[11] R. Dar, M. Feder, A. Mecozzi, and M. Shtaif, "Properties of nonlinear noise in long, dispersion-uncompensated fiber links," *Opt. Express*, vol. 21, no. 22, pp. 25 685–25 699, Nov 2013. [Online]. Available: http://www.opticsexpress.org/abstract.cfm?URI=oe-21-22-25685

[12] A. Carena, V. Curri, G. Bosco, P. Poggiolini, and F. Forghieri, "Modeling of the Impact of Nonlinear Propagation Effects in Uncompensated Optical Coherent Transmission Links," *J. Lightwave Technol.*, vol. 30, no. 10, pp. 1524–1539, May 2012. [Online]. Available: http://jlt.osa.org/abstract.cfm?URI=jlt-30-10-1524

[13] M. Secondini and E. Forestieri, "Analytical Fiber-Optic Channel Model in the Presence of Cross-Phase Modulation," *IEEE Photonics Technology Letters*, vol. 24, no. 22, pp. 2016–2019, Nov 2012.

[14] A. Mecozzi and R.-J. Essiambre, "Nonlinear Shannon Limit in Pseudolinear Coherent Systems," *J. Lightwave Technol.*, vol. 30, no. 12, pp. 2011–2024, Jun 2012. [Online]. Available: http://jlt.osa.org/abstract.cfm?URI=jlt-30-12-2011

[15] A. Bononi, P. Serena, N. Rossi, E. Grellier, and F. Vacondio, "Modeling nonlinearity in coherent transmissions with dominant intrachannel-four-wave-mixing," *Opt. Express*, vol. 20, no. 7, pp. 7777–7791, Mar 2012. [Online]. Available: http://www.opticsexpress.org/abstract.cfm?URI=oe-20-7-7777

[16] P. Serena and A. Bononi, "An Alternative Approach to the Gaussian Noise Model and its System Implications," *J. Lightwave Technol.*, vol. 31, no. 22, pp. 3489–3499, Nov 2013. [Online]. Available: http://jlt.osa.org/abstract.cfm?URI=jlt-31-22-3489

[17] P. Johannisson and M. Karlsson, "Perturbation Analysis of Nonlinear Propagation in a Strongly Dispersive Optical Communication System," *J. Lightw. Technol.*, vol. 31, no. 8, pp. 1273–1282, April 2013.

[18] P. Poggiolini, G. Bosco, A. Carena, V. Curri, Y. Jiang, and F. Forghieri, "The GN-Model of Fiber Non-Linear Propagation and its Applications," *J. Lightwave Technol.*, vol. 32, no. 4, pp. 694–721, Feb 2014. [Online]. Available: http://jlt.osa.org/abstract.cfm?URI=jlt-32-4-694

[19] OOPT_PSE. GNpy: Optical Route Planning Based on Gaussian Noise Model. [Online]. Available: https://github.com/Telecominfraproject/gnpy

[20] G. Rizzelli, G. Maier, M. Quagliotti, M. Schiano, and A. Pattavina, "Assessing the Scalability of Next-Generation Wavelength Switched Optical Networks," *Journal of Lightwave Technology*, vol. 32, no. 12, pp. 2263–2270, June 2014.

[21] S. Hardy, "Nokia upgrades 1830 PSS packet-optical transport family with new coherent chipsets, improved multi-rate performance," http://bit.ly/2zLYTv0, Mar. 2016.

[22] M. Cantono, J. L. Auge, and V. Curri, "Modelling the impact of SRS on NLI generation in commercial equipment: an experimental investigation," in *Submitted to Optical Fiber Communication Conference/National Fiber Optic Engineers Conference 2018*, 2018.

[23] M. Cantono, D. Pilori, A. Ferrari, and V. Curri, "Introducing the Generalized GN-model for Nonlinear Interference Generation including space/frequency variations of loss/gain," *arXiv preprint arXiv:1710.02225*, 2017.

[24] I. Roberts, J. M. Kahn, J. Harley, and D. W. Boertjes, "Channel Power Optimization of WDM Systems Following Gaussian Noise Nonlinearity Model in Presence of Stimulated Raman Scattering," *Journal of Lightwave Technology*, vol. 35, no. 23, pp. 5237–5249, Dec 2017.

[25] D. Semrau and P. Bayvel, "The Gaussian Noise Model in the Presence of Inter-channel Stimulated Raman Scattering," *arXiv preprint arXiv:1801.02460*, 2019.

[26] P. Poggiolini and Y. Jiang, "Recent Advances in the Modeling of the Impact of Nonlinear Fiber Propagation Effects on Uncompensated Coherent Transmission Systems," *Journal of Lightwave Technology*, vol. 35, no. 3, pp. 458–480, Feb 2017.

[27] D. Semrau, R. Killey, and P. Bayvel, "Achievable rate degradation of ultra-wideband coherent fiber communication systems due to stimulated Raman scattering," *Opt. Express*, vol. 25, no. 12, pp. 13 024–13 034, Jun 2017. [Online]. Available: http://www.opticsexpress.org/abstract.cfm?URI=oe-25-12-13024

[28] R. H. Stolen and E. P. Ippen, "Raman gain in glass optical waveguides," *Applied Physics Letters*, vol. 22, no. 6, pp. 276–278, 1973. [Online]. Available: http://scitation.aip.org/content/aip/journal/apl/22/6/10.1063/1.1654637

[29] G. Agrawal, "Nonlinear fiber optics," 2013.

[30] M. Cantono, V. Curri, A. Mecozzi, and R. Gaudino, "Polarization-Related Statistics of Raman Crosstalk in Single-Mode Optical Fibers," *Journal of Lightwave Technology*, vol. 34, no. 4, pp. 1191–1205, Feb 2016.

[31] C. R. S. Fludger, V. Handerek, and R. J. Mears, "Pump to signal RIN transfer in Raman fiber amplifiers," *Journal of Lightwave Technology*, vol. 19, no. 8, pp. 1140–1148, Aug 2001.

[32] M. Cantono, V. Curri, and R. Gaudino, "Raman Crosstalk Suppression in NG-PON2 Using Optimized Spectral Shaping," *J. Lightwave Technol.*, vol. 33, no. 24, pp. 5284–5292, Dec 2015. [Online]. Available: http://jlt.osa.org/abstract.cfm?URI=jlt-33-24-5284

[33] P. Poggiolini, G. Bosco, A. Carena, V. Curri, Y. Jiang, and F.Forghieri, "A detailed analytical derivation of the GN model of non-linear interference in coherent optical transmission systems," *arXiv preprint arXiv:1209.0394*, 2012.

[34] R. Dar, M. Feder, A. Mecozzi, and M. Shtaif, "Accumulation of nonlinear interference noise in fiber-optic systems," *Opt. Express*, vol. 22, no. 12, pp. 14 199–14 211, Jun 2014. [Online]. Available: http://www.opticsexpress.org/abstract.cfm?URI=oe-22-12-14199

[35] E. Pincemin, D. Grot, L. Bathany, S. Gosselin, M. Joindot, S. Bordais, Y. Jaouen, and J. Delavaux, "Raman gain efficiencies of modern terrestrial transmission fibers in s-, c- and l-band," in *Nonlinear Guided Waves and Their Applications*. Optical Society of America, 2002, p. NLTuC2. [Online]. Available: http://www.osapublishing.org/abstract.cfm?URI=NLGW-2002-NLTuC2

[36] D. Pilori, M. Cantono, A. Carena, and V. Curri, "FFSS: The fast fiber simulator software," in *Transparent Optical Networks (ICTON), 2017 19th International Conference on*. IEEE, 2017, pp. 1–4.